AMERICAN SOCIETY FOR MICROBIOLOGY | mBio®

RESEARCH ARTICLE
Molecular Biology and Physiology

High-Affinity Chemotaxis to Histamine Mediated by the TlpQ Chemoreceptor of the Human Pathogen *Pseudomonas aeruginosa*

Andrés Corral-Lugo,[a]* Miguel A. Matilla,[a] David Martín-Mora,[a] Hortencia Silva Jiménez,[a]* Noel Mesa Torres,[a] Junichi Kato,[b] Akiko Hida,[b] Shota Oku,[b] Mayte Conejero-Muriel,[c] Jose A. Gavira,[c] Tino Krell[a]

[a]Department of Environmental Protection, Estación Experimental del Zaidín, Consejo Superior de Investigaciones Científicas, Granada, Spain

[b]Department of Molecular Biotechnology, Graduate School of Advanced Sciences of Matter, Hiroshima University, Higashi-Hiroshima, Hiroshima, Japan

[c]Laboratory of Crystallographic Studies, IACT, (CSIC-UGR), Armilla, Spain

ABSTRACT Histamine is a key biological signaling molecule. It acts as a neurotransmitter in the central and peripheral nervous systems and coordinates local inflammatory responses by modulating the activity of different immune cells. During inflammatory processes, including bacterial infections, neutrophils stimulate the production and release of histamine. Here, we report that the opportunistic human pathogen *Pseudomonas aeruginosa* exhibits chemotaxis toward histamine. This chemotactic response is mediated by the concerted action of the TlpQ, PctA, and PctC chemoreceptors, which display differing sensitivities to histamine. Low concentrations of histamine were sufficient to activate TlpQ, which binds histamine with an affinity of 639 nM. To explore this binding, we resolved the high-resolution structure of the TlpQ ligand binding domain in complex with histamine. It has an unusually large dCACHE domain and binds histamine through a highly negatively charged pocket at its membrane distal module. Chemotaxis to histamine may play a role in the virulence of *P. aeruginosa* by recruiting cells at the infection site and consequently modulating the expression of quorum-sensing-dependent virulence genes. TlpQ is the first bacterial histamine receptor to be described and greatly differs from human histamine receptors, indicating that eukaryotes and bacteria have pursued different strategies for histamine recognition.

IMPORTANCE Genome analyses indicate that many bacteria possess an elevated number of chemoreceptors, suggesting that these species are able to perform chemotaxis to a wide variety of compounds. The scientific community is now only beginning to explore this diversity and to elucidate the corresponding physiological relevance. The discovery of histamine chemotaxis in the human pathogen *Pseudomonas aeruginosa* provides insight into tactic movements that occur within the host. Since histamine is released in response to bacterial pathogens, histamine chemotaxis may permit bacterial migration and accumulation at infection sites, potentially modulating, in turn, quorum-sensing-mediated processes and the expression of virulence genes. As a consequence, the modulation of histamine chemotaxis by signal analogues may result in alterations of the bacterial virulence. As the first report of bacterial histamine chemotaxis, this study lays the foundation for the exploration of the physiological relevance of histamine chemotaxis and its role in pathogenicity.

KEYWORDS *Pseudomonas aeruginosa*, chemotaxis, histamine

Received 30 August 2018 **Accepted** 12 October 2018 **Published** 13 November 2018

Citation Corral-Lugo A, Matilla MA, Martín-Mora D, Silva Jiménez H, Mesa Torres N, Kato J, Hida A, Oku S, Conejero-Muriel M, Gavira JA, Krell T. 2018. High-affinity chemotaxis to histamine mediated by the TlpQ chemoreceptor of the human pathogen *Pseudomonas aeruginosa*. mBio 9:e01894-18. https://doi.org/10.1128/mBio.01894-18.

Invited Editor Gerald L. Hazelbauer, University of Missouri-Columbia

Editor Tarek Msadek, Institut Pasteur

Address correspondence to Jose A. Gavira, jgavira@iact.ugr-csic.es, or Tino Krell, tino.krell@eez.csic.es.

* Present address: Andrés Corral-Lugo, Institut de Biologie Intégrative de la Cellule (I2BC), CNRS, Gif-Sur-Yvette, France; Hortencia Silva Jiménez, Instituto de Investigaciones Oceanológicas, Universidad Autónoma de Baja California, Ensenada, Baja California, México.

Bacteria possess different types of signal transduction systems that enable them to adapt to changes in environmental cues. In addition to one- and two-component signal transduction systems, chemosensory pathways play an important role in this process (1–3). In a canonical chemosensory pathway, signaling is initiated by the binding of signal molecules to the chemoreceptor ligand binding domain (LBD), which in turn modulates the autophosphorylation activity of the CheA histidine kinase and the transphosphorylation of the CheY response regulator, which ultimately triggers pathway output (2). While most chemoreceptors mediate chemotaxis, some also carry out alternative cellular functions, such as modulating c-di-GMP levels or type IV pilus-based motility (4–6).

Escherichia coli is the traditional model organism for the study of chemoreceptor-based signaling processes (7). It has 5 chemoreceptors, of which 4 contain a periplasmic 4-helix bundle LBD. Importantly, these chemoreceptors bind signals either directly or in complex with a periplasmic ligand binding protein. *E. coli* has a single chemosensory cascade that mediates chemotaxis primarily toward sugars, amino acids, or dipeptides (7, 8).

More recently, chemoreceptor-based signaling has been studied in an array of bacteria with different lifestyles (9). The existing data suggest that the typical number of chemoreceptor genes in bacteria, which can reach as high as 80, is much higher than in *E. coli* (10). Furthermore, sequence analyses indicate that chemoreceptors comprise more than eighty different LBD types (11). The most abundant of these are CACHE-type LBDs, which are present in either the monomodular (sCACHE) or bimodular (dCACHE) form (12). The large number of chemoreceptor genes and the diversity of LBD types suggest that bacteria can respond to a wide variety of signal molecules. The scientific community is now beginning to explore this diversity and to elucidate the corresponding physiological relevance.

Pseudomonads are important model organisms for the study of chemoreceptor function (13, 14), and the strains *Pseudomonas putida* KT2440 and *Pseudomonas aeruginosa* PAO1 have been well studied and characterized (11). The former strain is a nonpathogenic soil bacterium with a saprophytic lifestyle (15). In contrast, *P. aeruginosa* strains are among the most virulent opportunistic human pathogens and the leading cause of nosocomial infections, particularly in immunocompromised, cancer, burn, and cystic fibrosis patients (16).

Strains KT2440 and PAO1 have similar numbers of chemoreceptor genes: 27 and 26, respectively. The function and the corresponding ligand profiles have been established for approximately ten receptors in each strain (11, 17). Among the functionally annotated KT2440 chemotaxis receptors are several for different organic acids (18), purines (19), proteinogenic amino acids (20), and gamma-aminobutyric acid (GABA) (21). In addition, the McpU chemoreceptor of this strain was the first chemoreceptor identified that responded to the polyamines putrescine, spermidine, and cadaverine (20, 22). In contrast, PAO1 chemotaxis to proteinogenic amino acids and GABA is mediated by three paralogous receptors, namely, PctA, PctB, and PctC (23, 24). Additionally, this strain has two receptors for inorganic phosphate (25, 26) as well as receptors for malate (27, 28), α-ketoglutarate (29), and chloroethylenes (30). *P. aeruginosa* is also attracted to the plant hormone ethylene, and it was shown that the deletion of the gene encoding the TlpQ chemoreceptor abolished ethylene chemotaxis (31).

In this study, we provide the first report of bacterial chemotaxis toward histamine. This compound is produced by different animal tissues and is secreted by some bacteria (32). Histamine is a signal molecule with multiple functions. It is an aminergic neurotransmitter of the central and peripheral nervous systems, and it is involved in numerous biological processes (33). It is also a key modulator of local immune responses by mediating the effects on many cell types such as antigen-presenting cells, natural killer cells, and epithelial cells, as well as T and B lymphocytes (34). Bacteria have been shown to impact histamine function. For example, bacterial respiratory tract infections stimulate neutrophils to release histamine (35, 36). Also, it was shown that infection by PAO1 greatly increased neutrophil histamine content and secretion but did

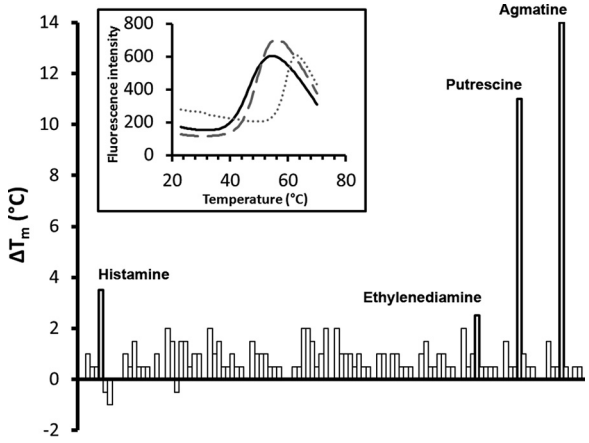

FIG 1 Thermal shift assays of *P. putida* KT2440 McpU-LBD against a library of ligands. Shown are the individual T_m changes caused by 95 compounds (Biolog array PM3B) that can serve as nitrogen sources. The inset shows the unfolding curves of McpU-LBD when free from ligand (continuous line) and in the presence of agmatine (dotted line) and histamine (dashed line).

not alter histamine production in mast cells, which are the classical histamine reservoirs (36). Furthermore, it has been shown that histamine might play divergent roles in the immune response: it has been implicated in mediating the defense against infection (37) as well as increasing the susceptibility to infection (38). While there has been preliminary evidence that histamine is a signal molecule for bacteria, the underlying mechanisms remain largely unknown (39). The present study provides important insight into the molecular mechanisms that permit bacteria to sense and respond to histamine.

RESULTS

Identification of histamine and additional polyamines as novel ligands for the *P. putida* KT2440 McpU chemoreceptor. By screening 190 compounds for binding to the purified McpU-LBD, we previously found that McpU binds to and mediates chemotaxis to putrescine, cadaverine, and spermidine (20). In the present study, we extended this screening to include 285 additional compounds. These compounds were mostly bacterial nitrogen, phosphorous, and sulfur sources (see Materials and Methods). We used a thermal shift assay to monitor changes in the midpoint of protein unfolding (T_m) caused by ligand binding (40). In the absence of ligand, McpU-LBD had a T_m of 46.5°C. Of the 95 nitrogen sources screened (Biolog plate PM3B), three additional compounds—agmatine, ethylenediamine, and histamine—caused T_m increases greater than 2°C (Fig. 1).

Using isothermal titration calorimetry (ITC), we found that all three compounds bind to McpU-LBD (see Fig. S1A in the supplemental material). Very tight binding was observed for agmatine with a K_D (equilibrium dissociation constant) in the nanomolar range, whereas histamine and ethylenediamine bound with much lower affinities (Table 1). It should be noted that of these three new McpU ligands and the previously identified ligands (i.e., putrescine, cadaverine, and spermidine), all except for histamine are polyamines (Fig. S1B).

Identification of TlpQ as a histamine receptor in *Pseudomonas aeruginosa*. Because histamine plays an important role in the immune response, we aimed to identify McpU homologues in *P. aeruginosa* that may also sense and mediate chemotaxis to histamine. To this end, we carried out a sequence clustering analysis of all dCACHE-containing chemoreceptors in PAO1 and KT2440 (see Fig. S2A). This analysis revealed that the LBD of the TlpQ receptor shares 62% sequence identity with the McpU-LBD homologue (Fig. S2B). To verify TlpQ function, we purified TlpQ-LBD for ITC binding studies. The results showed that five McpU-LBD ligands bind to TlpQ-LBD with nanomolar affinities, whereas the binding of ethylenediamine was slightly weaker

TABLE 1 Thermodynamic parameters for the binding of ligands to McpU-LBD and TlpQ-LBD as derived from ITC experiments[a]

	McpU-LBD		TlpQ-LBD		
Compound	**K_D (μM)**	**ΔH (kcal · mol^{-1})**	**K_D (nM)**	**ΔH (kcal · mol^{-1})**	**K_D McpU-LBD/K_D TlpQ-LBD**
Putrescine	2 ± 0.1[b]	−15 ± 0.5	134 ± 12	−6.8 ± 0.3	15
Cadaverine	22 ± 2[b]	−15.5 ± 0.5	150 ± 4	−6.0 ± 0.1	147
Spermidine	4.5 ± 0.4[b]	−4.3 ± 0.3	56 ± 4	−4.6± 0.4	80
Agmatine	0.48 ± 0.02	−14.5 ± 0.2	150 ± 9	−5.4 ± 0.1	3
Ethylenediamine	39 ± 4	−9.7 ± 0.5	1,710 ± 180	−6.3 ± 0.6	23
Histamine	26 ± 2	−2.6 ± 0.3	639 ± 27	−9.1 ± 0.3	41

[a]Means and standard deviations represent data from three independent experiments.
[b]Reported previously in reference 20.

(Fig. 2A, Table 1). Spermidine had a K_D of 56 nM, which is the highest ligand affinity ever observed for a chemoreceptor. Histamine had a K_D of 639 nM, which is an affinity 41 times higher than its affinity for McpU-LBD (Table 1, Fig. 2B). Thus, the affinities of the ligands to TlpQ-LBD were 3 to 147 times higher than their affinities to the McpU-LBD (Table 1). Previous studies showed that TlpQ mediates chemotaxis to ethylene (31), but the titration of TlpQ-LBD with a saturated ethylene solution did not show any binding (data not shown).

Characterization of histamine chemotaxis. KT2440 and PAO1 both contain chemoreceptors that bind histamine. In initial experiments, we identified the optimal culture conditions for motility of both strains (see Fig. S3). Using these conditions, we carried out capillary chemotaxis assays of PAO1 toward the six TlpQ ligands (Fig. 2C). All ligands caused chemotaxis, with significant responses observed for some ligands at concentrations as low as 500 nM, whereas optimal responses occurred at 5 mM. In subsequent experiments, we compared the histamine dose response for KT2440 with that of PAO1 (Fig. 3A). KT2440 showed only moderate chemotaxis over the entire concentration range tested, whereas PAO1 responses were much stronger. In accordance with the different binding affinities observed by ITC, the response onsets between strains also differed. Thus, PAO1 required 500 nM histamine, while KT2440 required 5 μM.

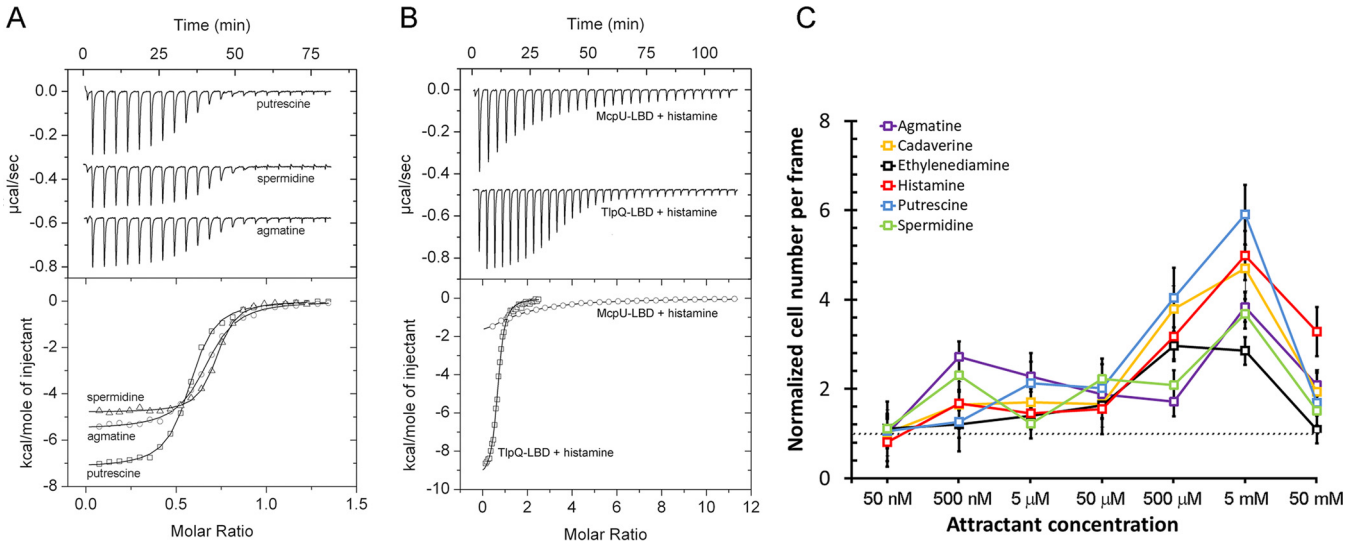

FIG 2 Identification and analysis of TlpQ ligands. (A) Microcalorimetric titrations of 15 μM TlpQ-LBD with 4.8 μl aliquots of 250 μM putrescine, spermidine, or cadaverine. (B) Microcalorimetric titration of 17.5 μM McpU-LBD with 9.6 μl aliquots of 1 mM histamine and titration of 15 μM TlpQ-LBD with 4.8 μl aliquots of 250 μM histamine. Upper graphs show raw titration data, while lower graphs show integrated corrected peak areas of the titration data fit using the "one binding site model." The derived thermodynamic parameters are provided in Table 1. (C) Quantitative capillary chemotaxis assays of *P. aeruginosa* PAO1 toward TlpQ ligands. Shown are the ratios of cells after 2 min of exposure to the chemoattractant relative to the number of cells at the beginning of the experiment. The horizontal line marks the ratio of 1, which is indicative of no chemotaxis; $n = 3$.

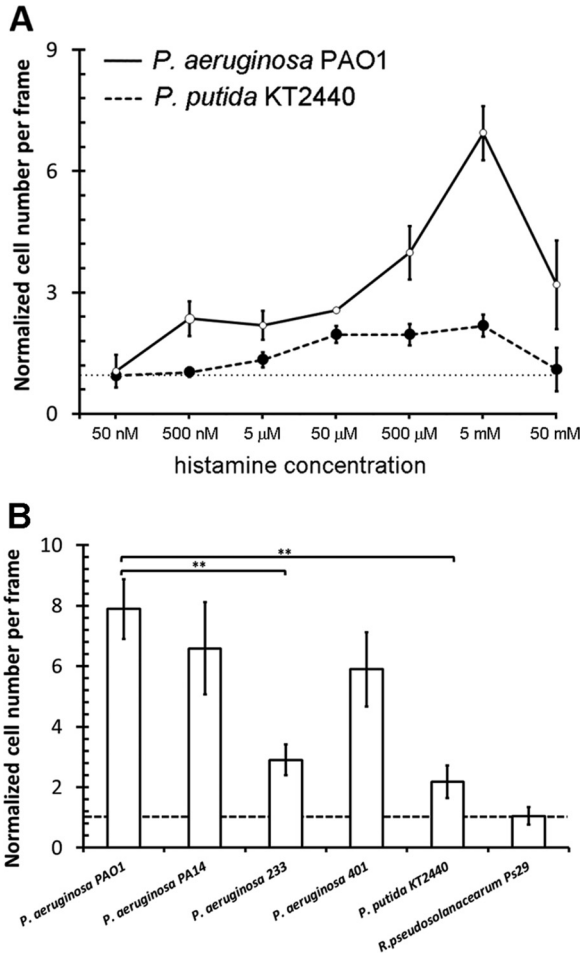

FIG 3 Histamine chemotaxis in different bacteria. (A) Quantitative capillary chemotaxis assays of *P. aeruginosa* PAO1 and *P. putida* KT2440 to different histamine concentrations. (B) Response of different strains to 5 mM histamine; $n = 3$. **, $P < 0.01$ (by Student's *t* tests).

To assess the metabolic value of these ligands, we conducted growth experiments with PAO1 and KT2440 in minimal medium containing each of the ligands as the sole carbon or nitrogen source. We found that most of the ligands supported growth either as the carbon or nitrogen source (see Fig. S4). The exceptions were spermidine and ethylenediamine that were either not or were poor growth substrates for PAO1 and KT2440 (Fig. S4). Histamine permitted the growth of both strains as the sole C and N source.

Additional experiments were conducted to assess histamine chemotaxis in other bacteria. First, we assessed the motility of *P. aeruginosa* strains 227, 233, 287, 401, and 428, which were isolated from patients with urinary tract infections (41). Strains 233 and 401 exhibited motilities comparable to that of PAO1 and were therefore selected for further studies. *P. aeruginosa* PA14 as well as the plant pathogen *Ralstonia pseudosolanacearum* Ps29 were also included in these experiments. We found that all analyzed *P. aeruginosa* strains showed significant chemotaxis to 5 mM histamine, and their chemotactic phenotype was significantly higher than that of KT2440. On the other hand, the strain Ps29 was not attracted to histamine (Fig. 3B). Growth experiments with Ps29 in minimal medium containing histamine as the sole carbon and nitrogen source revealed no significant growth (Fig. S4B), suggesting a link between chemotaxis and the capacity to use histamine for growth.

Three-dimensional structure of TlpQ-LBD in complex with histamine. To determine the molecular determinants for histamine recognition by TlpQ, we solved the

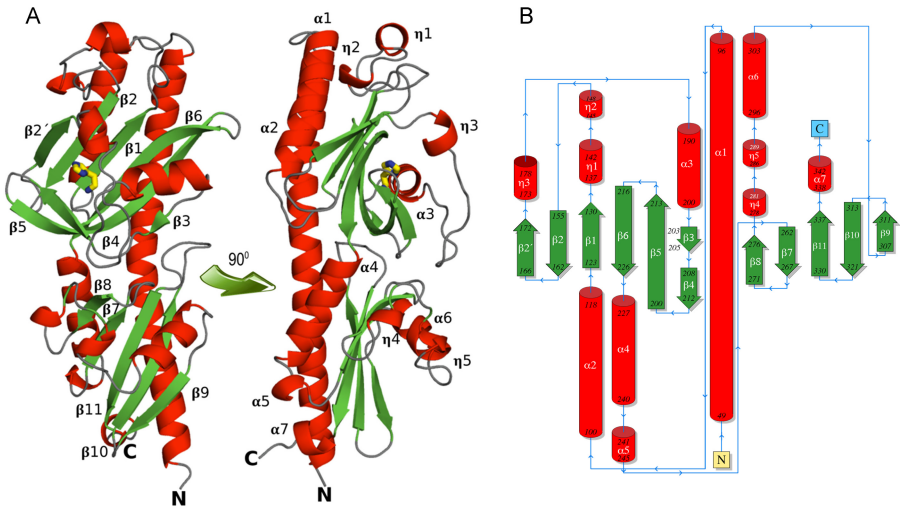

FIG 4 Structure of the TlpQ chemoreceptor ligand binding domain in complex with histamine. (A) Ribbon diagram with annotated secondary structure elements. Bound histamine is shown as a stick structure. (B) Schematic representation of the secondary structure elements.

high-resolution structure of TlpQ-LBD in complex with histamine. There are four monomers in the asymmetric unit,and the superimposition of their C_α atoms resulted in root mean square deviation (RMSD) values of 0.4 to 0.8 Å, indicative of high similarity. An inspection of the structure revealed that it is a dCACHE domain (12) (Fig. 4). A long N-terminal helix is followed by two globular α/β modules, termed membrane-proximal and membrane-distal modules. The membrane-distal module contained bound histamine in all four monomers of the asymmetric unit (Fig. 4).

Structural alignments of TlpQ-LBD with entries in the protein data bank identified structural homologues (see Table S1). Most of the homologues are categorized as dCACHE_1 Pfam domains (12). This domain is found in histidine kinases and chemoreceptors, as well as in a novel cytosolic receptor protein (PDB identifier [ID] 5ere), and are found in different bacteria as well as in *Arabidopsis*. The average size of the domains, while taking into account the segment in between both transmembrane regions, is 268 ± 17 amino acids (Table S1). Of all the homologous domains that we identified, TlpQ-LBD was the largest, at 334 amino acids, namely due to particularly long inserts between β-strands 1 and 2, extended helices α1 and α2, and an extended loop between helices η3 and α3 (see Fig. S5).

A well-defined electron density for histamine was observed in all four monomers, enabling the ligand placement to be determined (Fig. 5A). TlpQ ligands are present as protonated polycations at neutral pH, which explains why the ligand binding pocket is highly negatively charged (Fig. 5B). All three histamine nitrogen atoms establish hydrogen bonds (Fig. 5C). TlpQ ligands contain at least one primary amino group, and the primary amino group of histamine plays a central role in binding because it forms hydrogen bonds with the side chains of Tyr208, Asp210, and Asp239. In addition, this histamine amino group interacts with a water molecule coordinated by the main chain oxygen of Lys211 and the hydroxyl group of Tyr158. Each of the histamine imidazole nitrogen atoms forms hydrogen bonds with Asp210 and Glu170. The LBDs of TlpQ and McpU of *P. putida* KT2440 share approximately 50% sequence identity (Fig. S2B). When their structures containing either histamine or putrescine were superimposed (Fig. 5D), it became apparent that the primary amino groups of both ligands are coordinated in a similar manner via hydrogen bonds with Y208/D210/D239 of TlpQ-LBD or their equivalents in McpU-LBD.

Histamine chemotaxis is mediated by multiple chemoreceptors in PAO1. To assess the role of TlpQ in histamine chemotaxis, we generated a *tlpQ* mutant. Control experiments showed that its response to Casamino Acids was comparable to that of the

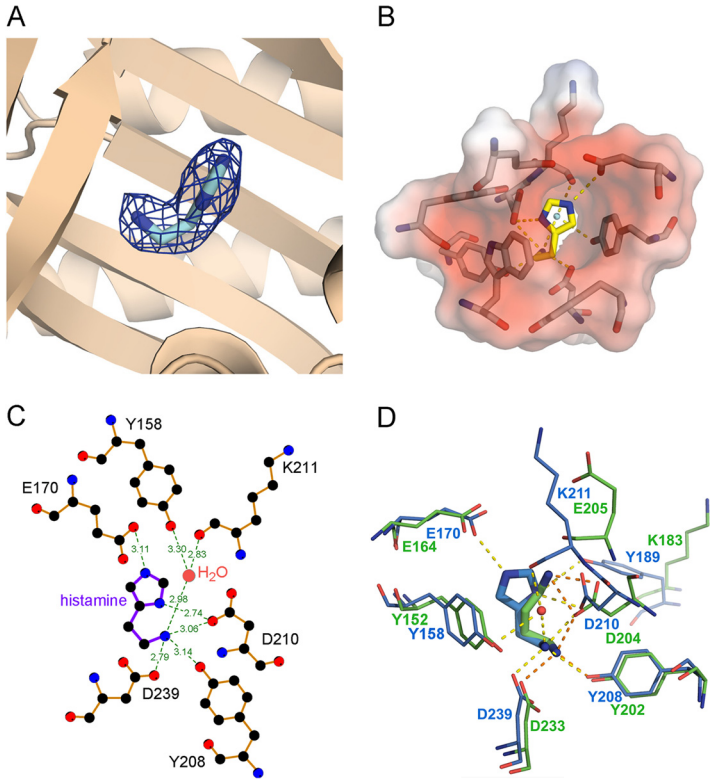

FIG 5 Ligand binding pocket of the TlpQ ligand binding domain. (A) Close-up view of the ligand binding pocket. The electron density for histamine is shown. (B) Surface charge representation of the histamine binding site; red and blue shading represent negative and positive charges, respectively. (C) Schematic representation of amino acids involved in hydrogen bonds with histamine. (D) Superimposition of the ligand binding pockets of McpU-LBD with bound putrescine (green, PDB ID 6F9G) and TlpQ-LBD with bound histamine (blue).

wild type. However, the response of this mutant to 5 mM histamine was also similar to that of the wild type (Fig. 6A), indicating that additional chemoreceptors may be involved.

To identify these additional chemoreceptors, we screened a number of mutants, in which 3 to 7 chemoreceptor genes had been deleted. Our results showed that the deletion of the *pctA*, *pctB*, and *pctC* chemoreceptor genes (strain PCT2) abolished chemotaxis to 5 mM histamine (Fig. 6A). PctA, PctB, and PctC are chemoreceptors for L-amino acids (23, 24), while PctC also mediates chemotaxis toward GABA (21).

To clarify the roles of PctA, PctB, PctC, and TlpQ in histamine chemotaxis, we conducted dose-response experiments using wild-type PCT2 as well as a mutant in which the *pctABC* as well as the *tlpQ* gene had been deleted, named PCT2Q (Fig. 6B). The latter mutant was devoid of histamine chemotaxis over the entire concentration range (50 nM to 50 mM), whereas significant chemotaxis was observed for the PCT2 mutant at a concentration range between 500 nM and 500 μM. This indicates that TlpQ mediates chemotaxis to low histamine concentrations, which is in agreement with the very high affinity observed *in vitro*. In contrast, one or more of the PctA, PctB, and PctC receptors mediate chemotaxis to elevated histamine concentrations.

To assess the role of the individual chemoreceptors, the PCT2Q mutant devoid of histamine chemotaxis was complemented with plasmids containing one of the four chemoreceptors—an approach that has previously proven effective to study complex chemotactic processes (42). To confirm the phenotypes of these strains, chemotaxis was measured toward previously identified ligands, namely L-Ile (PctA), L-Arg (PctB), and GABA (PctC) (23, 24), and the three complemented strains responded to these ligands. Histamine chemotaxis measurements revealed that the *pctC* and *tlpQ* genes in *trans*

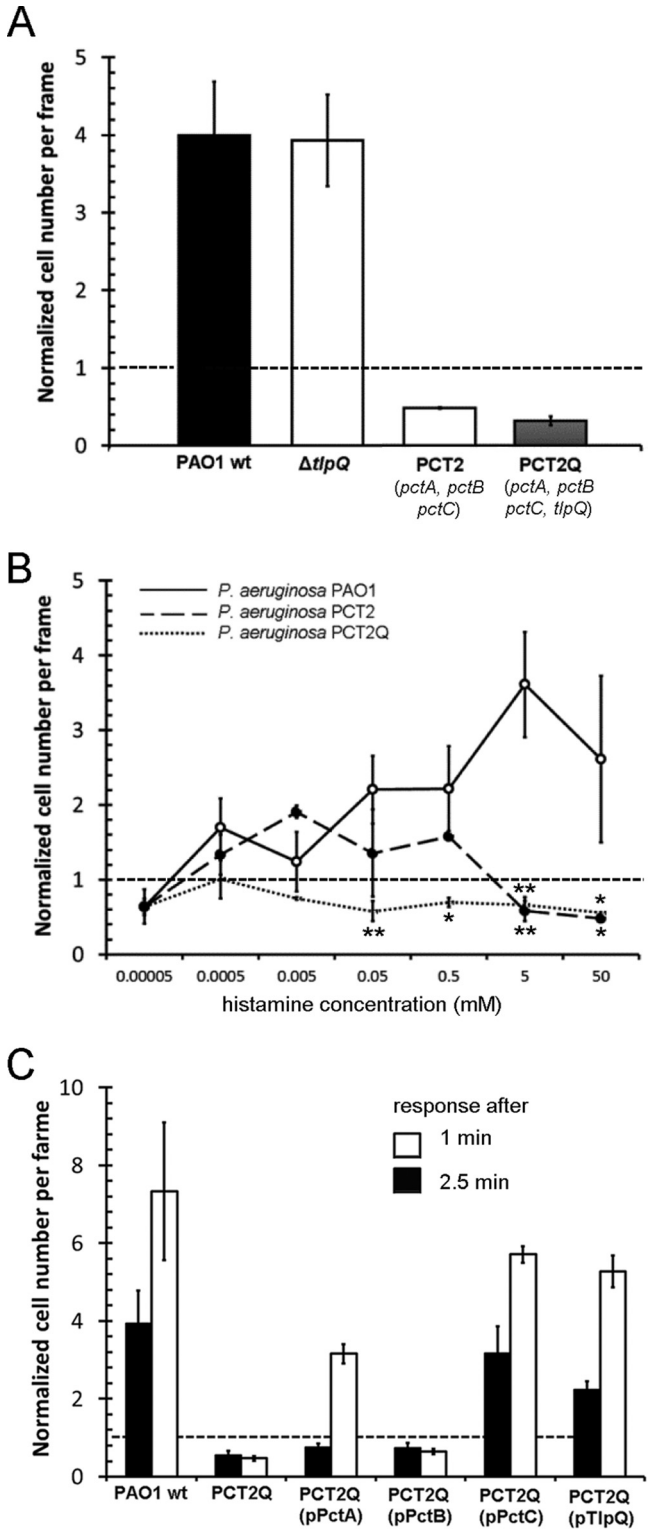

FIG 6 Chemotaxis to histamine is mediated by multiple chemoreceptors in *P. aeruginosa* PAO1. (A) Chemotactic responses to 5 mM histamine by wild-type and mutant strains. (B) Histamine dose-response chemotaxis assays for PAO1 and for PCT2 and PCT2Q mutants. (C) Chemotactic response of PAO1 and PCT2Q harboring plasmids pPctA, pPctB, pPctC, and pTlpQ to 500 μM histamine after contact times of 1 min and 2.5 min; $n = 3$. *, $P < 0.05$; **, $P < 0.01$ (by Student's t tests).

recovered histamine chemotaxis using an exposure time of 1 min. At 2.5 min, complementation with *pctA*, *pctC*, and *tlpQ* resulted in significant chemotaxis (Fig. 6C). Thus, these data reveal that histamine chemotaxis is mediated by the concerted action of PctA, PctC, and TlpQ. To assess the role of these receptors in another strain, we generated a triple mutant in the homologous receptors of *P. aeruginosa* PA14. As shown in Fig. S6, the deletion of these receptors also abolished histamine chemotaxis.

TlpQ, PctA, and PctC employ different mechanisms to mediate histamine chemotaxis. To determine the mechanism by which PctA and PctC respond to histamine, microcalorimetric binding studies with purified PctA-LBD and PctC-LBD were conducted. Whereas the proteins bound L-Ala and L-Gln (24), respectively, histamine did not bind. Direct microcalorimetric titrations can only provide information on high-affinity binding events because of the limitations presented by ligand dilution heats. To assess the possibility of low-affinity histamine binding, we conducted a competition assay. PctA-LBD was titrated with L-Ala in the presence and absence of 20 mM histamine. However, the resulting titration curves were almost identical (see Fig. S7), confirming that histamine does not bind directly to PctA-LBD.

To assess whether PctA and PctC may be activated by histamine-containing periplasmic binding proteins, pulldown experiments with immobilized PctA-LBD and PctC-LBD as well as PAO1 protein extracts were conducted using previously verified protocols (25). However, our results provided no evidence for binding partners to either domain.

DISCUSSION

The elevated numbers of chemoreceptors in many bacteria suggest that this abundance confers chemotactic capabilities to many different stimuli, and the scientific community is only beginning to explore the diversity of these responses. In general, chemoeffectors can be classified into three groups according to their physiological role. First, the majority of chemoattractants are important nutritional sources, as evidenced by numerous receptors that respond to different organic or amino acids (11). Second, chemoattraction has been observed for signal molecules such as plant hormones (31, 43), neurotransmitters (44), and quorum sensing signals (45), which inform bacteria about their environment. Lastly, chemoreceptors can signal the presence of compounds, such as histamine, that are involved in multiple functions.

Thus, what is the physiological relevance of chemotaxis toward histamine? One possibility is certainly that, like most of the other McpU/TlpQ ligands, histamine supports growth as the sole C and N source. However, chemotaxis to host signals has been shown for many different pathogens to be essential for efficient infection and virulence (46). Importantly, *P. aeruginosa* PAO1 was shown to greatly increase neutrophil histamine content and secretion in mouse models (36), and chemotaxis to this host-derived signal will result in an accumulation of bacterial cells at the infection site. This increase in bacterial cell density likely alters the expression of quorum-sensing-controlled genes, including those responsible for the production of virulence determinants and biofilm formation in *P. aeruginosa* (47). Nonetheless, the precise assessment of the role of histamine chemotaxis in the virulence of *P. aeruginosa* is technically a difficult undertaking, since it is unfeasible to generate a mutant that is deficient in histamine chemotaxis without impairing taxis to the remaining identified ligands for PctA (17 amino acids), PctC (GABA and 2 amino acids), and TlpQ (5 polyamines) (24).

The interference with motility and chemotaxis is an alternative strategy to block bacterial pathogens (48). Previous work has shown that some chemoreceptors recognize chemoattractants and antagonists (27, 49, 50), and the identification of antagonists that specifically interfere with histamine chemotaxis may thus be an alternative approach to modulate the virulence properties of *P. aeruginosa*. Remarkably, the identification of these antagonists may be facilitated by the resolution of the three-dimensional structure of TlpQ-LBD in complex with histamine (Fig. 4 and 5).

High sensitivity histamine responses are mediated by the TlpQ chemoreceptor, which binds histamine directly. TlpQ is in many aspects an atypical chemoreceptor.

First, its LBD, which is 334 amino acids, is larger than any other known chemoreceptor LBD (11). Second, it has the highest affinity ever observed for the binding of a chemoattractant to the recombinant LBD of a chemoreceptor. Histamine binding occurred with an affinity of 639 nM, which is among the highest affinities observed for chemoattractants. This unusually high affinity permits responses to very low histamine concentrations, and the onset of chemotactic response occurred at the unusually low concentration of 500 nM (Fig. 2C).

Frequently, the deletion of a chemoreceptor abolishes taxis to a given compound, indicating that there is a single receptor for a given chemoattractant (18, 29). However, histamine chemotaxis is mediated by the concerted action of three receptors. Thus, what is the advantage of having multiple receptors for the same chemoattractant? In this context, close similarities exist between histamine chemotaxis and the mechanisms by which *P. aeruginosa* is attracted to inorganic phosphate (P_i). P_i is a key signaling molecule that controls the expression of many virulence genes (51, 52). Chemotaxis to a low P_i concentration is mediated by the CtpL receptor, whereas CtpH is responsible for responses to high concentrations (25, 26). Whereas CtpH recognizes P_i directly at its LBD, CtpL is stimulated by the P_i-loaded periplasmic binding protein PstS (25). A chemoreceptor, either stimulated by direct or indirect signal recognition, is characterized by a response range (53). The combined action of multiple chemoreceptors with different sensing abilities permits the microorganism to expand its response range to a given chemoattractant. The presence of multiple receptors for a given chemoeffector may suggest that a compound is particularly physiologically relevant.

Four human histamine receptors have been described, termed H1, H2, H3, and H4 (54). Histamine was shown to mediate the chemotaxis of mast cells via the H4 receptor, and this mechanism might be responsible for mast cell accumulation in allergic tissues (55). However, the topology of eukaryotic histamine receptors differs entirely from that of their bacterial counterparts. All four receptor types form a barrel composed of seven transmembrane helices (54). The three-dimensional structure of the human H1 receptor has been solved (56), which revealed that ligands bind within this transmembrane barrel. Therefore, the evolutionary strategies to sense histamine greatly differ between bacteria and humans.

Here, we provide the first report of bacterial chemotaxis toward histamine. Histamine is vital to cellular processes in mammals, and the initial evidence suggests that histamine also functions as a bacterial signal molecule. This study expands the range of known bacterial chemoeffectors and lays the foundation for deciphering the molecular mechanisms underlying histamine chemotaxis and its role in bacterial virulence.

MATERIALS AND METHODS

Bacterial strains and plasmids. The bacterial strains and plasmids used are listed in Table 2, and oligonucleotides are listed in Table S2 in the supplemental material.

Construction of bacterial mutant strains and plasmids. The *pctA* and *tlpQ* genes were deleted in different mutant strains by unmarked gene deletion. Plasmids pK18*mobsacB-pctA* and pK18*mobsacB-tlpQ* were generated by amplifying 0.6- to 1.2-kb regions up- and downstream of the target gene. PCR products were digested with the restriction enzymes listed in Table S2 and cloned into pK18*mobsacB*. The resulting plasmids were introduced into *E. coli* S17-1 λ*pir* by electroporation. Plasmids were transferred to PAO1 by conjugation, and cells were selected in Simmons citrate (BBL; Becton, Dickinson) agar plates supplemented with kanamycin. For plasmid excision, LB medium was inoculated with a kanamycin-resistant colony and grown for 12 h, and then spread on LB plates containing 20% (wt/vol) sucrose. To construct the triple deletion mutant in *pctA*, *pctC*, and *tlpQ* in *P. aeruginosa* PA14, pK18*mobsacB-pctA* and pK18*mobsacB-tlpQ* were consecutively conjugated into PA14 to generate the double mutant. Subsequently, the plasmid pK18*mobsacB-pctC*, generated by amplifying regions up- and downstream of *pctC*, was conjugated into PA14 Δ*pctA* Δ*tlpQ*. Kanamycin-resistant colonies were grown on LB agar plates supplemented with 20% (wt/vol) sucrose for selection. For complementation purposes, the *pctC* gene was amplified by PCR and cloned into plasmid pUCP18 using the restriction enzymes listed in Table S2. The ligation mixture was electroporated into *E. coli* JM109, and transformants were selected on carbenicillin-containing LB plates. The resulting plasmid pPctC was transferred to PCTC1 and PCT2Q by electroporation.

Construction of the TlpQ-LBD expression plasmid. The DNA fragment encoding the LBD of TlpQ was amplified, digested with NdeI and BamHI, and cloned into pET28b(+) linearized with the same enzymes.

TABLE 2 Bacterial strains and plasmids used in this study

Strain or plasmid	Characteristics[1]	Reference or source
Strains		
Escherichia coli BL21(DE3)	F$^-$ *ompI hsdS*$_B$(r$_B^-$ m$_B^-$) *gal dam met*	69
DH5α	*supE44 lacU169*(φ80*lacZ*ΔM15) *hsdR17* (r$_K^-$ m$_K^-$) *recA1 endA1 gyrA96 thi-1 relA1*	70
HB101	F$^-$ Δ(*gpt-proA*)*62 leuB6 supE44 ara-14 galK2 lacY1* Δ(*mcrC-mrr*) *rpsL20* (Sm^r) *xyl-5 mtl-1 recA13 thi-1*	71
JM109	F′ *traD36 proA*$^+$*B*$^+$ *lacI*^{q} Δ(*lacZ*)M15 Δ(*lac-proAB*) *glnV44 e14*$^-$ *gyrA96 recA1 relA1 endA1 thi hsdR17*	72
S17-1 λ*pir*	Tp^r Sm^r (*rec*A *thi pro hsdR*)$^-$ M+*RP4*: 2-Tc:Mu: Km Tn*7* λ*pir*	73
Ralstonia pseudosolanacearum Ps29	Wild-type strain race 1, biovar 3, phylotype I	74
Pseudomonas putida KT2440	Wild type	15
KT2440R	Rifampicin-resistant derivative of KT2440	75
KT2440R-McpU	KT2440R transposon mutant *pp1228*::mini-Tn*5*-Km; Rif^r, Km^r	76
Pseudomonas aeruginosa PAO1	Wild-type strain	77
PAO1 Δ*pctA*	PAO1 derivative, *pctA* gene deletion mutant	This study
PCTB1	PAO1 derivative, *pctB*::Km; Km^r	23
PCTC1	PAO1 derivative, *pctC*::Km; Km^r	23
PAO1 Δ*tlpQ*	PAO1 derivative, *pa2654* gene deletion mutant	This study
PCT2	PAO1 derivative; Δ*pctB-pctA-pa4308-pctC*::km; Km^r[b]	23
PCTAQ	PAO1 derivative; Δ*pctA* Δ*tlpQ*	This study
PCT2Q	PAO1 derivative; Δ*pctB-pctA-pa4308-pctC*::Km, Δ*tlpQ*; Km^r	This study
PCT2QP	PAO1 derivative; Δ*pctB-pctA-pa4308-pctC*::Km, Δ*tlpQ* Δ*tlpP*; Km^r	J. Kato lab
PCT2QART	PAO1 derivative; Δ*pctB-pctA-pa4308-pctC*, Δ*tlpQ* Δ*tlpA* (*pa1646*), Δ*tlpR*(*pa2652*) Δ*tlpT*(*pa1930*); Km^r	J. Kato lab
P. aeruginosa PA14	Wild-type strain; human clinical isolate that elicits disease in plants, nematodes, insects, and mice	78
PA14-ACQ	PA14 derivative; Δ*pctA* Δ*pctC* Δ*tlpQ* Δ*pa4308*	This study
P. aeruginosa isolate 227	Isolated clinical strain from patients with urinary tract infections	41
P. aeruginosa isolate 233	Isolated clinical strain from patients with urinary tract infections	41
P. aeruginosa isolate 287	Isolated clinical strain from patients with urinary tract infections	41
P. aeruginosa isolate 401	Isolated clinical strain from patients with urinary tract infections	41
P. aeruginosa isolate 428	Isolated clinical strain from patients with urinary tract infections	41
Plasmids		
pUCP18	*Escherichia-Pseudomonas* shuttle vector; Ap^r	79
pPctA	pUCP18 with a PCR fragment containing *pctA*; Ap^r	80
pPctB	pUCP18 with a PCR fragment containing *pctB*; Ap^r	80
pPctC	pUCP18 with a PCR fragment containing *pctC*; Ap^r	This study
pTlpQ	pUCP18 with a PCR fragment containing *tlpQ*; Ap^r	27
pK18*mobsacB*	Plasmid for allelic exchange; pK18 *ori*$V_{E.C}$*lacZ*α *mob sacB*; Km^r	81
pK18*mobsacB-pctA*	pK18*mobsacB* containing a deletion of the *pctA* gene; Km^r	This study
pK18*mobsacB-tlpQ*	pK18*mobsacB* containing a deletion of the *tlpQ* gene; Km^r	This study
pK18*mobsacB-pctABC*	pK18*mobsacB* containing a deletion of *pctB*, *pctA*, *pa4308*, *pctC*; Km^r	This study
pK18*mobsacB-pctC*	pK18*mobsacB* containing a deletion of *pctC* and *pa4308*; Km^r	This study
pET28b(+)	Protein expression plasmid; Km^r	Novagen
pET28b-McpU	pET28b derivative used to produce His-tagged McpU-LBD; Km^r	20
pET28b-TlpQ	pET28b derivative used to produce His-tagged TlpQ-LBD; Km^r	This study

[a]Ap, ampicillin; Km, kanamycin; Rif, rifampin.
[b]The *pa4308* gene (orf-1), which forms part of the *pctABC* operon, encodes a hypothetical protein that is not involved in chemotaxis (23).

Overexpression and purification of proteins. PctA-LBD and PctC-LBD were overexpressed and purified as described in reference 24. McpU-LBD and TlpQ-LBD were generated as reported in reference 20.

Thermal shift assay. Thermal shift experiments were conducted as reported in reference in 57. McpU-LBD in polybuffer {5 mM Tris, 5 mM PIPES [piperazine-*N*,*N*′-bis(2-ethanesulfonic acid)], 5 mM MES [morpholineethanesulfonic acid], 10% glycerol [vol/vol], 150 mM NaCl, pH 7.0} was used at a final concentration of 10 μM. Biolog (Hayward, CA, USA) compound arrays PM3B (nitrogen sources), PM4A (phosphorous and sulfur sources), and PM5 (nutrient supplements) were used for screening. The compositions of these arrays are provided at http://208.106.130.253/pdf/pm_lit/PM1-PM10.pdf.

Isothermal titration calorimetry. Titrations were carried out in a VP microcalorimeter (MicroCal, Northampton, MA, USA) at 25°C. Proteins dialyzed into polybuffer were titrated with ligands in dialysis buffer. Typically, 15 to 30 μM protein was titrated with 0.25 to 1 mM ligand solutions. For ethylene binding studies, TlpQ-LBD was titrated with 12-μl aliquots of a saturated ethylene solution in polybuffer, prepared as reported in reference 31. The mean enthalpies from the injection of ligands into the buffer were subtracted from titration data prior to data fitting using the "one binding site model" of ORIGIN.

Chemotaxis assays. (i) Soft agar plate assays. Strains were grown overnight in M9 minimal medium containing 0.1% glucose (wt/vol), diluted to an optical density at 600 nm (OD$_{660}$) of 1 with fresh

medium, and washed twice with M9 medium. The pellet was resuspended in 1 ml M9 medium. Ten-microliter aliquots of 5 mM chemoattractant solutions were placed onto plates containing M9 medium, 2.5 mM glucose, and 0.25% (wt/vol) agar. Two-microliter aliquots of bacterial suspensions were placed horizontally to each of the chemoattractant spots. The plates were incubated at 30°C for 16 to 20 h.

(ii) Quantitative capillary chemotaxis assays. Two protocols were used that differed in the ways the cells were counted. The first protocol was used to generate the data shown Fig. S6, whereas the second protocol was used for the remaining chemotaxis experiments. In the first protocol, overnight cultures of strains were diluted to an OD_{660} of 0.05 in MS medium (58) supplemented with 6 mg·liter^{-1} Fe citrate, trace elements, and 15 mM glucose and grown at 37°C. At an OD_{660} of 0.4, the cultures were centrifuged at 1,700 × *g* for 5 min and the pellet was washed twice with chemotaxis buffer (50 mM potassium phosphate, 20 mM EDTA, 0.05% [vol/vol] glycerol, pH 7.0). The cells were resuspended in this buffer and adjusted to an OD_{660} of 0.1, and 230-μl aliquots were placed into 96-well plates. Capillary tubes (P1424, Microcaps; Drummond Scientific) were heat sealed at one end and filled with chemotaxis buffer or chemotaxis chemoattractant solution. The capillaries were then immersed in bacterial suspensions at their open ends. After 30 min at room temperature, the capillaries were removed and rinsed with sterile water, and the content was expelled into 1 ml of M9 medium. Serial dilutions were plated on LB medium, and the CFU were determined. In all cases, the data were corrected to the number of cells that swam into the buffer-containing capillaries. In the second protocol, we used computer-assisted image analysis as reported previously (59). Briefly, capillaries were filled with chemoattractant solutions in 10 mM HEPES buffer (pH 7.0) containing 1% (wt/vol) agarose and heat sealed on one side. The cells were grown in 2× yeast extract-tryptone (YT), medium and 10-μl aliquots of the cell suspension were placed onto a microscope slide within the U-shaped spacer, which was then covered by a coverslip. The chemoattractant-filled capillaries were introduced into the chemotaxis chamber, and cell movement was videotaped, with images taken at the beginning and at different time intervals. If not otherwise stated, the contact time between the cell and the chemoattractant was 2 min. The Bioinformatics Assistant Icy Sport detector software (60) was used to determine the number of cells per image. The magnitude of chemotaxis was expressed as the number of cells after a given time over the number of cells at the beginning of the experiment. The data shown are the means and standard deviations from three experiments conducted in triplicates.

Growth experiments. PAO1 was grown overnight in MS minimal medium (29) containing 20 mM D-glucose. Cultures were diluted to an OD_{600} of 0.02 in MS medium supplemented with 5 mM carbon or nitrogen source. The assays were performed in 100-well polystyrene plates and incubated at 30°C (KT2440) or 37°C (PAO1) in a Bioscreen microbiological growth analyzer. The data represent the means and standard deviations from three biological replicates conducted in triplicates.

Assessment of motility. To assess bacterial motility, PAO1 and KT2440 were used to inoculate LB and 2× YT medium to an OD_{600} of 0.01. Growth was carried out at 37°C (PAO1) or 30°C (KT2440), and the bacteria were inspected microscopically. According to their motility, they were given different scores: score 1, 25% of bacteria are motile; 2, 50%; 3, 75%; and 4, 100%.

Crystallization and structure resolution. Crystallization trials were carried out with TlpQ-LBD in the absence and presence of histamine. TlpQ-LBD in polybuffer was incubated with a 2-fold molar excess of histamine on ice for 30 min. Unbound ligand was removed by buffer exchange using 10-kDa-cutoff filters (Amicon) and polybuffer. The apo- (6 mg/ml) and ligand-bound (26 mg/ml) proteins were loaded into 0.3-mm-diameter capillaries for counter diffusion crystallization using screen kits from Triana S & T (Granada, Spain). Only the LBD-TlpQ–histamine complex produced crystals in 1.5 M ammonium phosphate and 0.1 M sodium citrate pH 5.6. The same protocol was used to crystallize the Se-Met TlpQ-LBD. The capillaries were emptied into mother solution containing 10% to 25% (vol/vol) glycerol as the cryoprotectant. Crystals were diffracted at the European Synchrotron Radiation Facility and the Spanish Synchrotron ALBA. The data were indexed and integrated with XDS (61) and scaled with SCALA (62). All attempts to obtain a molecular replacement solution failed. Phases were obtained from the Se-methionine derivative by combining SAD data, at the selenium peak, with an initial model generated by Phyre2 (63), as input files for Auto-Rickshaw (64). All 26 expected heavy atom positions were identified by SHELXD (65) using the data to 3.5 Å. The model generated was refined with phenix.refine (66). Further refinement was performed against the best data set (2.45 Å) with phenix.refine (66) using Coot (67). Model quality was checked using MolProbity (68). The refinement statistics and quality indicators of the final model are summarized in Table S3. The structure was deposited at the protein data bank with identifier (ID) 6fu4.

SUPPLEMENTAL MATERIAL

Supplemental material for this article may be found at https://doi.org/10.1128/mBio.01894-18.

FIG S1, JPG file, 0.6 MB.
FIG S2, TIF file, 1.1 MB.
FIG S3, TIF file, 0.1 MB.
FIG S4, JPG file, 0.7 MB.
FIG S5, JPG file, 0.7 MB.
FIG S6, TIF file, 1.4 MB.
FIG S7, JPG file, 0.2 MB.

TABLE S1, DOCX file, 0.03 MB.
TABLE S2, DOCX file, 0.02 MB.
TABLE S3, DOCX file, 0.01 MB.

ACKNOWLEDGMENTS

We acknowledge the European Synchrotron Radiation Facility (beamlines ID23-1 & 2, ID30B, and ID30A-3) and the Spanish Synchrotron ALBA (beamline XALOC) and thank the staff for their invaluable support.

This work was supported by FEDER funds and Fondo Social Europeo through grants held by T. Krell from the Spanish Ministry for Economy and Competitiveness (grants BIO2013-42297 and BIO2016-76779-P) and by grant BIO2016-74875-P to J. A. Gavira.

REFERENCES

1. Galperin MY. 2005. A census of membrane-bound and intracellular signal transduction proteins in bacteria: bacterial IQ, extroverts and introverts. BMC Microbiol 5:35. https://doi.org/10.1186/1471-2180-5-35.
2. Hazelbauer GL, Falke JJ, Parkinson JS. 2008. Bacterial chemoreceptors: high-performance signaling in networked arrays. Trends Biochem Sci 33:9–19. https://doi.org/10.1016/j.tibs.2007.09.014.
3. Laub MT, Goulian M. 2007. Specificity in two-component signal transduction pathways. Annu Rev Genet 41:121–145. https://doi.org/10.1146/annurev.genet.41.042007.170548.
4. Wuichet K, Zhulin IB. 2010. Origins and diversification of a complex signal transduction system in prokaryotes. Sci Signal 3:ra50. https://doi.org/10.1126/scisignal.2000724.
5. Hickman JW, Tifrea DF, Harwood CS. 2005. A chemosensory system that regulates biofilm formation through modulation of cyclic diguanylate levels. Proc Natl Acad Sci U S A 102:14422–14427. https://doi.org/10.1073/pnas.0507170102.
6. Whitchurch CB, Leech AJ, Young MD, Kennedy D, Sargent JL, Bertrand JJ, Semmler AB, Mellick AS, Martin PR, Alm RA, Hobbs M, Beatson SA, Huang B, Nguyen L, Commolli JC, Engel JN, Darzins A, Mattick JS. 2004. Characterization of a complex chemosensory signal transduction system which controls twitching motility in *Pseudomonas aeruginosa*. Mol Microbiol 52:873–893. https://doi.org/10.1111/j.1365-2958.2004.04026.x.
7. Parkinson JS, Hazelbauer GL, Falke JJ. 2015. Signaling and sensory adaptation in *Escherichia coli* chemoreceptors: 2015 update. Trends Microbiol 23:257–266. https://doi.org/10.1016/j.tim.2015.03.003.
8. Matilla MA, Krell T. 2017. Chemoreceptor-based signal sensing. Curr Opin Biotechnol 45:8–14. https://doi.org/10.1016/j.copbio.2016.11.021.
9. Bardy SL, Briegel A, Rainville S, Krell T. 2017. Recent advances and future prospects in bacterial and archaeal locomotion and signal transduction. J Bacteriol 199:e00203-17. https://doi.org/10.1128/JB.00203-17.
10. Alexandre G, Greer-Phillips S, Zhulin IB. 2004. Ecological role of energy taxis in microorganisms. FEMS Microbiol Rev 28:113–126. https://doi.org/10.1016/j.femsre.2003.10.003.
11. Ortega A, Zhulin IB, Krell T. 2017. Sensory repertoire of bacterial chemoreceptors. Microbiol Mol Biol Rev 81:e00033-17. https://doi.org/10.1128/MMBR.00033-17.
12. Upadhyay AA, Fleetwood AD, Adebali O, Finn RD, Zhulin IB. 2016. Cache domains that are homologous to, but different from PAS domains comprise the largest superfamily of extracellular sensors in prokaryotes. PLoS Comput Biol 12:e1004862. https://doi.org/10.1371/journal.pcbi.1004862.
13. Sampedro I, Parales RE, Krell T, Hill JE. 2015. *Pseudomonas* chemotaxis. FEMS Microbiol Rev 39:17–46. https://doi.org/10.1111/1574-6976.12081.
14. Kato J, Kim HE, Takiguchi N, Kuroda A, Ohtake H. 2008. *Pseudomonas aeruginosa* as a model microorganism for investigation of chemotactic behaviors in ecosystem. J Biosci Bioeng 106:1–7. https://doi.org/10.1263/jbb.106.1.
15. Belda E, van Heck RGA, José Lopez-Sanchez M, Cruveiller S, Barbe V, Fraser C, Klenk H-P, Petersen J, Morgat A, Nikel PI, Vallenet D, Rouy Z, Sekowska A, Martins dos Santos VAP, de Lorenzo V, Danchin A, Médigue C. 2016. The revisited genome of *Pseudomonas putida* KT2440 enlightens its value as a robust metabolic chassis. Environ Microbiol 18:3403–3424. https://doi.org/10.1111/1462-2920.13230.
16. Juhas M. 2015. *Pseudomonas aeruginosa* essentials: an update on investigation of essential genes. Microbiology 161:2053–2060. https://doi.org/10.1099/mic.0.000161.
17. Ortega DR, Fleetwood AD, Krell T, Harwood CS, Jensen GJ, Zhulin IB. 2017. Assigning chemoreceptors to chemosensory pathways in *Pseudomonas aeruginosa*. Proc Natl Acad Sci U S A 114:12809–12814. https://doi.org/10.1073/pnas.1708842114.
18. Garcia V, Reyes-Darias JA, Martin-Mora D, Morel B, Matilla MA, Krell T. 2015. Identification of a chemoreceptor for C2 and C3 carboxylic acids. Appl Environ Microbiol 81:5449–5457. https://doi.org/10.1128/AEM.01529-15.
19. Fernandez M, Morel B, Corral-Lugo A, Krell T. 2016. Identification of a chemoreceptor that specifically mediates chemotaxis toward metabolizable purine derivatives. Mol Microbiol 99:34–42. https://doi.org/10.1111/mmi.13215.
20. Corral-Lugo A, De la Torre J, Matilla MA, Fernández M, Morel B, Espinosa-Urgel M, Krell T. 2016. Assessment of the contribution of chemoreceptor-based signaling to biofilm formation. Environ Microbiol 18:3355–3372. https://doi.org/10.1111/1462-2920.13170.
21. Reyes-Darias JA, García V, Rico-Jiménez M, Corral-Lugo A, Lesouhaitier O, Juárez-Hernández D, Yang Y, Bi S, Feuilloley M, Muñoz-Rojas J, Sourjik V, Krell T. 2015. Specific gamma-aminobutyrate chemotaxis in *pseudomonads* with different lifestyle. Mol Microbiol 97:488–501. https://doi.org/10.1111/mmi.13045.
22. Gavira JA, Ortega A, Martín-Mora D, Conejero-Muriel MT, Corral-Lugo A, Morel B, Matilla MA, Krell T. 2018. Structural basis for polyamine binding at the dCACHE domain of the McpU chemoreceptor from *Pseudomonas putida*. J Mol Biol 430:1950–1963. https://doi.org/10.1016/j.jmb.2018.05.008.
23. Taguchi K, Fukutomi H, Kuroda A, Kato J, Ohtake H. 1997. Genetic identification of chemotactic transducers for amino acids in *Pseudomonas aeruginosa*. Microbiology 143:3223–3229. https://doi.org/10.1099/00221287-143-10-3223.
24. Rico-Jimenez M, Munoz-Martinez F, Garcia-Fontana C, Fernandez M, Morel B, Ortega A, Ramos JL, Krell T. 2013. Paralogous chemoreceptors mediate chemotaxis towards protein amino acids and the non-protein amino acid gamma-aminobutyrate (GABA). Mol Microbiol 88:1230–1243. https://doi.org/10.1111/mmi.12255.
25. Rico-Jiménez M, Reyes-Darias JA, Ortega Á, Díez Peña AI, Morel B, Krell T. 2016. Two different mechanisms mediate chemotaxis to inorganic phosphate in *Pseudomonas aeruginosa*. Sci Rep 6:28967. https://doi.org/10.1038/srep28967.
26. Wu H, Kato J, Kuroda A, Ikeda T, Takiguchi N, Ohtake H. 2000. Identification and characterization of two chemotactic transducers for inorganic phosphate in *Pseudomonas aeruginosa*. J Bacteriol 182:3400–3404. https://doi.org/10.1128/JB.182.12.3400-3404.2000.
27. Martin-Mora D, Ortega A, Perez-Maldonado FJ, Krell T, Matilla MA. 2018. The activity of the C4-dicarboxylic acid chemoreceptor of *Pseudomonas aeruginosa* is controlled by chemoattractants and antagonists. Sci Rep 8:2102. https://doi.org/10.1038/s41598-018-20283-7.
28. Alvarez-Ortega C, Harwood CS. 2007. Identification of a malate chemoreceptor in *Pseudomonas aeruginosa* by screening for chemotaxis defects in an energy taxis-deficient mutant. Appl Environ Microbiol 73:7793–7795. https://doi.org/10.1128/AEM.01898-07.
29. Martin-Mora D, Ortega A, Reyes-Darias JA, García V, López-Farfán D, Matilla MA, Krell T. 2016. Identification of a chemoreceptor in *Pseudomonas aeruginosa* that specifically mediates chemotaxis towards alpha-ketoglutarate. Front Microbiol 7:1937. https://doi.org/10.3389/fmicb.2016.01937.

30. Kim HE, Shitashiro M, Kuroda A, Takiguchi N, Ohtake H, Kato J. 2006. Identification and characterization of the chemotactic transducer in *Pseudomonas aeruginosa* PAO1 for positive chemotaxis to trichloroethylene. J Bacteriol 188:6700–6702. https://doi.org/10.1128/JB.00584-06.
31. Kim H-E, Shitashiro M, Kuroda A, Takiguchi N, Kato J. 2007. Ethylene chemotaxis in *Pseudomonas aeruginosa* and other *Pseudomonas* species. Microb Environ 22:186–189. https://doi.org/10.1264/jsme2.22.186.
32. Barcik W, Wawrzyniak M, Akdis CA, O'Mahony L. 2017. Immune regulation by histamine and histamine-secreting bacteria. Curr Opin Immunol 48:108–113. https://doi.org/10.1016/j.coi.2017.08.011.
33. De Benedetto A, Yoshida T, Fridy S, Park JE, Kuo IH, Beck LA. 2015. Histamine and skin barrier: are histamine antagonists useful for the prevention or treatment of atopic dermatitis? J Clin Med 4:741–755. https://doi.org/10.3390/jcm4040741.
34. O'Mahony L, Akdis M, Akdis CA. 2011. Regulation of the immune response and inflammation by histamine and histamine receptors. J Allergy Clin Immunol 128:1153–1162. https://doi.org/10.1016/j.jaci.2011.06.051.
35. Xu X, Zhang D, Zhang H, Wolters PJ, Killeen NP, Sullivan BM, Locksley RM, Lowell CA, Caughey GH. 2006. Neutrophil histamine contributes to inflammation in mycoplasma pneumonia. J Exp Med 203:2907–2917. https://doi.org/10.1084/jem.20061232.
36. Xu X, Zhang H, Song Y, Lynch SV, Lowell CA, Wiener-Kronish JP, Caughey GH. 2012. Strain-dependent induction of neutrophil histamine production and cell death by *Pseudomonas aeruginosa*. J Leukoc Biol 91:275–284. https://doi.org/10.1189/jlb.0711356.
37. Metz M, Doyle E, Bindslev-Jensen C, Watanabe T, Zuberbier T, Maurer M. 2011. Effects of antihistamines on innate immune responses to severe bacterial infection in mice. Int Arch Allergy Immunol 155:355–360. https://doi.org/10.1159/000321614.
38. Beghdadi W, Porcherie A, Schneider BS, Dubayle D, Peronet R, Huerre M, Watanabe T, Ohtsu H, Louis J, Mecheri S. 2008. Inhibition of histamine-mediated signaling confers significant protection against severe malaria in mouse models of disease. J Exp Med 205:395–408. https://doi.org/10.1084/jem.20071548.
39. Kyriakidis DA, Theodorou MC, Tiligada E. 2012. Histamine in two component system-mediated bacterial signaling. Front Biosci (Landmark ed) 17:1108–1119.
40. Krell T. 2015. Tackling the bottleneck in bacterial signal transduction research: high-throughput identification of signal molecules. Mol Microbiol 96:685–688. https://doi.org/10.1111/mmi.12975.
41. Oura H, Tashiro Y, Toyofuku M, Ueda K, Kiyokawa T, Ito S, Takahashi Y, Lee S, Nojiri H, Nakajima-Kambe T, Uchiyama H, Futamata H, Nomura N. 2015. Inhibition of *Pseudomonas aeruginosa* swarming motility by 1-naphthol and other bicyclic compounds bearing hydroxyl groups. Appl Environ Microbiol 81:2808–2818. https://doi.org/10.1128/AEM.04220-14.
42. Ni B, Huang Z, Fan Z, Jiang CY, Liu SJ. 2013. *Comamonas testosteroni* uses a chemoreceptor for tricarboxylic acid cycle intermediates to trigger chemotactic responses towards aromatic compounds. Mol Microbiol 90:813–823. https://doi.org/10.1111/mmi.12400.
43. Antunez-Lamas M, Cabrera E, Lopez-Solanilla E, Solano R, Gonzalez-Melendi P, Chico JM, Toth I, Birch P, Pritchard L, Liu H, Rodriguez-Palenzuela P. 2009. Bacterial chemoattraction towards jasmonate plays a role in the entry of *Dickeya dadantii* through wounded tissues. Mol Microbiol 74:662–671. https://doi.org/10.1111/j.1365-2958.2009.06888.x.
44. Pasupuleti S, Sule N, Cohn WB, MacKenzie DS, Jayaraman A, Manson MD. 2014. Chemotaxis of *Escherichia coli* to norepinephrine (NE) requires conversion of NE to 3,4-dihydroxymandelic acid. J Bacteriol 196:3992–4000. https://doi.org/10.1128/JB.02065-14.
45. Laganenka L, Colin R, Sourjik V. 2016. Chemotaxis towards autoinducer 2 mediates autoaggregation in Escherichia coli. Nat Commun 7:12984. https://doi.org/10.1038/ncomms12984.
46. Matilla MA, Krell T. 2018. The effect of bacterial chemotaxis on host infection and pathogenicity. FEMS Microbiol Rev 42:fux052. https://doi.org/10.1093/femsre/fux052.
47. Azam MW, Khan AU. 20 July 2018. Updates on the pathogenicity status of *Pseudomonas aeruginosa*. Drug Discov Today https://doi.org/10.1016/j.drudis.2018.07.003.
48. Erhardt M. 2016. Strategies to block bacterial pathogenesis by interference with motility and chemotaxis. Curr Top Microbiol Immunol 398:185–205. https://doi.org/10.1007/82_2016_493.
49. Bi S, Yu D, Si G, Luo C, Li T, Ouyang Q, Jakovljevic V, Sourjik V, Tu Y, Lai L. 2013. Discovery of novel chemoeffectors and rational design of *Escherichia coli* chemoreceptor specificity. Proc Natl Acad Sci U S A 110:16814–16819. https://doi.org/10.1073/pnas.1306811110.
50. Yu D, Ma X, Tu Y, Lai L. 2015. Both piston-like and rotational motions are present in bacterial chemoreceptor signaling. Sci Rep 5:8640. https://doi.org/10.1038/srep08640.
51. Bains M, Fernandez L, Hancock RE. 2012. Phosphate starvation promotes swarming motility and cytotoxicity of *Pseudomonas aeruginosa*. Appl Environ Microbiol 78:6762–6768. https://doi.org/10.1128/AEM.01015-12.
52. Zaborin A, Romanowski K, Gerdes S, Holbrook C, Lepine F, Long J, Poroyko V, Diggle SP, Wilke A, Righetti K, Morozova I, Babrowski T, Liu DC, Zaborina O, Alverdy JC. 2009. Red death in *Caenorhabditis elegans* caused by *Pseudomonas aeruginosa* PAO1. Proc Natl Acad Sci U S A 106:6327–6332. https://doi.org/10.1073/pnas.0813199106.
53. Neumann S, Hansen CH, Wingreen NS, Sourjik V. 2010. Differences in signalling by directly and indirectly binding ligands in bacterial chemotaxis. EMBO J 29:3484–3495. https://doi.org/10.1038/emboj.2010.224.
54. Panula P, Chazot PL, Cowart M, Gutzmer R, Leurs R, Liu WL, Stark H, Thurmond RL, Haas HL. 2015. International Union of Basic and Clinical Pharmacology. XCVIII. Histamine receptors. Pharmacol Rev 67:601–655. https://doi.org/10.1124/pr.114.010249.
55. Hofstra CL, Desai PJ, Thurmond RL, Fung-Leung WP. 2003. Histamine H4 receptor mediates chemotaxis and calcium mobilization of mast cells. J Pharmacol Exp Ther 305:1212–1221. https://doi.org/10.1124/jpet.102.046581.
56. Shimamura T, Shiroishi M, Weyand S, Tsujimoto H, Winter G, Katritch V, Abagyan R, Cherezov V, Liu W, Han GW, Kobayashi T, Stevens RC, Iwata S. 2011. Structure of the human histamine H1 receptor complex with doxepin. Nature 475:65–70. https://doi.org/10.1038/nature10236.
57. Fernandez M, Ortega A, Rico-Jimenez M, Martin-Mora D, Daddaoua A, Matilla MA, Krell T. 2018. High-throughput screening to identify chemoreceptor ligands. Methods Mol Biol 1729:291–301. https://doi.org/10.1007/978-1-4939-7577-8_23.
58. Abril MA, Michan C, Timmis KN, Ramos JL. 1989. Regulator and enzyme specificities of the TOL plasmid-encoded upper pathway for degradation of aromatic hydrocarbons and expansion of the substrate range of the pathway. J Bacteriol 171:6782–6790. https://doi.org/10.1128/jb.171.12.6782-6790.1989.
59. Nikata T, Sumida K, Kato J, Ohtake H. 1992. Rapid method for analyzing bacterial behavioral responses to chemical stimuli. Appl Environ Microbiol 58:2250–2254.
60. de Chaumont F, Dallongeville S, Chenouard N, Herve N, Pop S, Provoost T, Meas-Yedid V, Pankajakshan P, Lecomte T, Le Montagner Y, Lagache T, Dufour A, Olivo-Marin JC. 2012. Icy: an open bioimage informatics platform for extended reproducible research. Nat Methods 9:690–696. https://doi.org/10.1038/nmeth.2075.
61. Kabsch W. 2010. XDS. Acta Crystallogr D Biol Crystallogr 66:125–132. https://doi.org/10.1107/S0907444909047337.
62. Evans P. 2006. Scaling and assessment of data quality. Acta Crystallogr D Biol Crystallogr 62:72–82. https://doi.org/10.1107/S0907444905036693.
63. Kelley LA, Sternberg MJ. 2009. Protein structure prediction on the Web: a case study using the Phyre server. Nat Protoc 4:363–371. https://doi.org/10.1038/nprot.2009.2.
64. Panjikar S, Parthasarathy V, Lamzin VS, Weiss MS, Tucker PA. 2005. Auto-rickshaw: an automated crystal structure determination platform as an efficient tool for the validation of an X-ray diffraction experiment. Acta Crystallogr D Biol Crystallogr 61:449–457. https://doi.org/10.1107/S0907444905001307.
65. Schneider TR, Sheldrick GM. 2002. Substructure solution with SHELXD. Acta Crystallogr D Biol Crystallogr 58:1772–1779. https://doi.org/10.1107/S0907444902011678.
66. Afonine PV, Mustyakimov M, Grosse-Kunstleve RW, Moriarty NW, Langan P, Adams PD. 2010. Joint X-ray and neutron refinement with phenix.refine. Acta Crystallogr D Biol Crystallogr 66:1153–1163. https://doi.org/10.1107/S0907444910026582.
67. Emsley P, Lohkamp B, Scott WG, Cowtan K. 2010. Features and development of Coot. Acta Crystallogr D Biol Crystallogr 66:486–501. https://doi.org/10.1107/S0907444910007493.
68. Chen VB, Arendall WB, III, Headd JJ, Keedy DA, Immormino RM, Kapral GJ, Murray LW, Richardson JS, Richardson DC. 2010. MolProbity: all-atom structure validation for macromolecular crystallography. Acta Crystallogr D Biol Crystallogr 66:12–21. https://doi.org/10.1107/S0907444909042073.
69. Jeong H, Barbe V, Lee CH, Vallenet D, Yu DS, Choi SH, Couloux A, Lee SW, Yoon SH, Cattolico L, Hur CG, Park HS, Segurens B, Kim SC, Oh TK, Lenski

RE, Studier FW, Daegelen P, Kim JF. 2009. Genome sequences of *Escherichia coli* B strains REL606 and BL21(DE3). J Mol Biol 394:644–652. https://doi.org/10.1016/j.jmb.2009.09.052.
70. Woodcock DM, Crowther PJ, Doherty J, Jefferson S, DeCruz E, Noyer-Weidner M, Smith SS, Michael MZ, Graham MW. 1989. Quantitative evaluation of *Escherichia coli* host strains for tolerance to cytosine methylation in plasmid and phage recombinants. Nucleic Acids Res 17:3469–3478. https://doi.org/10.1093/nar/17.9.3469.
71. Boyer HW, Roulland-Dussoix D. 1969. A complementation analysis of the restriction and modification of DNA in *Escherichia coli*. J Mol Biol 41:459–472. https://doi.org/10.1016/0022-2836(69)90288-5.
72. Zylstra GJ, Wackett LP, Gibson DT. 1989. Trichloroethylene degradation by *Escherichia coli* containing the cloned *Pseudomonas putida* F1 toluene dioxygenase genes. Appl Environ Microbiol 55:3162–3166.
73. Phornphisutthimas S, Thamchaipenet A, Panijpan B. 2007. Conjugation in *Escherichia coli*: a laboratory exercise. Biochem Mol Biol Educ 35:440–445. https://doi.org/10.1002/bmb.113.
74. Hida A, Oku S, Kawasaki T, Nakashimada Y, Tajima T, Kato J. 2015. Identification of the *mcpA* and *mcpM* genes, encoding methyl-accepting proteins involved in amino acid and l-malate chemotaxis, and involvement of McpM-mediated chemotaxis in plant infection by *Ralstonia pseudosolanacearum* (formerly *Ralstonia solanacearum* phylotypes I and III). Appl Environ Microbiol 81:7420–7430. https://doi.org/10.1128/AEM.01870-15.
75. Espinosa-Urgel M, Ramos JL. 2004. Cell density-dependent gene contributes to efficient seed colonization by *Pseudomonas putida* KT2440. Appl Environ Microbiol 70:5190–5198. https://doi.org/10.1128/AEM.70.9.5190-5198.2004.
76. Duque E, Molina-Henares AJ, de la Torre J, Molina-Henares MA, del Castillo T, Lam J, Ramos JL. 2007. Towards a genome-wide mutant library of *Pseudomonas putida* strain KT2440, p 227–251. *In* Ramos JL, Filloux A (ed), Pseudomonas: a model system in biology, volV. Springer, Dorchester, the Netherlands.
77. Holloway BW, Krishnapillai V, Morgan AF. 1979. Chromosomal genetics of *Pseudomonas*. Microbiol Rev 43:73–102.
78. Rahme LG, Stevens EJ, Wolfort SF, Shao J, Tompkins RG, Ausubel FM. 1995. Common virulence factors for bacterial pathogenicity in plants and animals. Science 268:1899–1902. https://doi.org/10.1126/science.7604262.
79. Schweizer HP. 1991. *Escherichia-Pseudomonas* shuttle vectors derived from pUC18/19. Gene 97:109–121. https://doi.org/10.1016/0378-1119(91)90016-5.
80. Shitashiro M, Tanaka H, Hong CS, Kuroda A, Takiguchi N, Ohtake H, Kato J. 2005. Identification of chemosensory proteins for trichloroethylene in *Pseudomonas aeruginosa*. J Biosci Bioeng 99:396–402. https://doi.org/10.1263/jbb.99.396.
81. Schafer A, Tauch A, Jager W, Kalinowski J, Thierbach G, Puhler A. 1994. Small mobilizable multi-purpose cloning vectors derived from the *Escherichia coli* plasmids pK18 and pK19: selection of defined deletions in the chromosome of *Corynebacterium glutamicum*. Gene 145:69–73. https://doi.org/10.1016/0378-1119(94)90324-7.